Neurochemical Research (2019) 44:374–387
https://doi.org/10.1007/s11064-018-2684-7

ORIGINAL PAPER

Impaired Cerebellar Development in Mice Overexpressing VGF

Takahiro Mizoguchi[1] · Masamitsu Shimazawa[1] · Kazuki Ohuchi[1] · Yoshiki Kuse[1] · Shinsuke Nakamura[1] · Hideaki Hara[1]

Received: 31 July 2018 / Revised: 9 November 2018 / Accepted: 15 November 2018 / Published online: 20 November 2018

Abstract
VGF nerve growth factor inducible (VGF) is a neuropeptide precursor induced by brain-derived neurotrophic factor and nerve growth factor. VGF is increased in the prefrontal cortex and cerebrospinal fluid in schizophrenia patients. In our previous study, VGF-overexpressing mice exhibited schizophrenia-like behaviors and smaller brain weights. Brain developmental abnormality is one cause of mental illness. Research on brain development is important for discovery of pathogenesis of mental disorders. In the present study, we investigated the role of VGF on cerebellar development. We performed a histological analysis with cerebellar sections of adult and postnatal day 3 mice by Nissl staining. To investigate cerebellar development, we performed immunostaining with antibodies of immature and mature granule cell markers. To understand the mechanism underlying these histological changes, we examined MAPK, Wnt, and sonic hedgehog signaling by Western blot. Finally, we performed rotarod and footprint tests using adult mice to investigate motor function. VGF-overexpressing adult mice exhibited smaller cerebellar sagittal section area. In postnatal day 3 mice, a cerebellar sagittal section area reduction of the whole cerebellum and external granule layer and a decrease in the number of mature granule cells were found in VGF-overexpressing mice. Additionally, the number of proliferative granule cell precursors was lower in VGF-overexpressing mice. Phosphorylation of Trk and Erk1 were increased in the cerebellum of postnatal day 3 VGF-overexpressing mice. Adult VGF-overexpressing mice exhibited motor disability. All together, these findings implicate VGF in the development of cerebellar granule cells via promoting MAPK signaling and motor function in the adult stage.

Keywords VGF nerve growth factor inducible · Neural development · Cerebellum · Granule cell · Motor coordination

Introduction

VGF nerve growth factor inducible (VGF) is a peptide precursor that is processed into biologically active peptides including TLQP-62, TLQP-21, and AQEE-30 [1, 2]. VGF was first identified as a nerve growth factor (NGF)-induced protein in PC12 cells [3]. Later studies demonstrated that VGF is induced by other neurotrophic factors, including brain-derived neurotrophic factor (BDNF) and neurotrophin-3 (NT-3) in primary cultures of cortical and hippocampal neurons [4, 5]. The effects of VGF are implicated in BDNF/TrkB signaling, and VGF promotes the phosphorylation of TrkB [6–8].

The human *VGF* gene is located on chromosome 7q22.1, on which copy number variants (CNVs) are reported in patients with schizophrenia [9, 10]. Moreover, patients with schizophrenia and depression have higher levels of VGF [11, 12]. Previous reports suggest that the upregulation of VGF may be implicated in the pathology of mental disorders, especially schizophrenia. We reported on generating the mice that overexpress VGF (VGF-overexpressing mice) and investigated several behavioral phenotypes [13, 14]. VGF-overexpressing mice exhibited some schizophrenia-related phenotypes and responsiveness to antipsychotics [13, 14].

Developmental disability of the brain is implicated in the pathology of several mental disorders, including schizophrenia and autism [15–17]. Developmental abnormalities of neural cells and circuits are caused by both genetic and environmental factors [18–22]. Neuroimaging research has revealed a broad hypoplasia of several brain regions, including the cerebellum, hippocampus, cerebral cortex, and striatum in patients with mental disorders [23, 24]. Evidence

✉ Hideaki Hara
hidehara@gifu-pu.ac.jp

[1] Molecular Pharmacology, Department of Biofunctional Evaluation, Gifu Pharmaceutical University, 1-25-4 Daigaku-Nishi, Gifu 501-1196, Japan

indicates that growth factors and cytokines may be involved in neuronal development [25–28]. In previous reports, VGF enhanced neurogenesis in cultured hippocampal neurons, and promoted dendritic growth of cultured cortical neurons [7, 29, 30]. However, how VGF influences the development of the immature brain in vivo is still unknown.

The cerebellum is involved in the neural control of motor movement, emotion, and cognition [31, 32]. The development of cerebellum is well investigated in several studies [33–35]. The cerebellum is easy to investigate in studies of brain development [36]. The reasons are following. (1) The cerebellum is at an independent position from other brain regions. (2) The time of cerebellar development is later than other brain regions. (3) The cerebellar laminar structure is simple with few cells, including Purkinje cells, granule cells, Bergmann glia, several interneurons, and deep cerebellar nuclei. Therefore, the cerebellum is suitable to study the role of VGF on the development of the brain. Our aim in this study was to investigate the roles of VGF in cerebellar neuronal development.

Materials and Methods

Animals

VGF-overexpressing mice (BDF1 mice) were generated as previously reported [13]. Wild-type (WT) and VGF-overexpressing mice were generated by heterozygous VGF-overexpressing mice and BDF1 mice (SLC, Shizuoka, Japan). The male animals (8–18-weeks-old) were housed at 24 °C under a 12 h light–dark cycle (lights on 8:00–20:00) with ad libitum access to food and water. All procedures relating to animal care were approved and monitored by the Institutional Animal Care and Use Committee of Gifu Pharmaceutical University and were performed after approval by the Bioethics and Biosafety Committee of Gifu Pharmaceutical University. All efforts were made to minimize suffering and the number of animals used. All procedures relating to animal care conformed to animal care guidelines issued by the National Institutes of Health. We used WT littermates as a control group. All behavioral experiments were performed on 9:00–20:00.

Western Blot Analysis

Each naive mouse was decapitated, and its brain was quickly removed and placed on a cooled plate, where the cerebella of VGF-overexpressing mice and WT mice were rapidly dissected. The tissue was lysed in ice-cold tissue lysis buffer [50 mM Tris–HCl (pH 8.0) containing 150 mM NaCl, 50 mM EDTA, 1% Triton X-100 (Bio-Rad Labs, Hercules, CA, USA) and protease/phosphatase inhibitor (Sigma-Aldrich, St. Louis, MO, USA)]. The tissue was homogenized using a homogenizer (Microtec, Funabashi, Japan). The lysate was centrifuged at 10,000 rpm for 20 min, and the supernatant was collected for use in the experiments. The protein concentration was determined by comparison with known concentrations of bovine serum albumin using a BCA Protein Assay kit (Thermo Fisher Scientific, Waltham, MA, USA). Lysates were solubilized in sodium dodecyl sulfate sample buffer, separated on a 5–20% sodium dodecyl sulfate–polyacrylamide gradient gel, and transferred to a membrane. The membranes were blocked for 30 min at room temperature with Blocking One P (Nakarai Tesque, Kyoto, Japan). After blocking, the membranes were washed in 10 mM Tris-buffered saline with 0.05% Tween20 and then incubated at 4 °C with the primary antibody. The membranes were washed in 10 mM Tris-buffered saline with 0.05% Tween20; incubated at room temperature in a secondary antibody; and visualized using a digital imaging system (LAS-4000UV mini; Fujifilm, Tokyo, Japan). The primary antibodies used were goat polyclonal anti-VGF (sc-10383; Santa Cruz Biotechnology, Dallas, TX, USA), rabbit monoclonal anti-phospho-p44/42 MAPK (Erk1/2) (#4377; Cell Signaling Technology, Danvers, MA, USA), rabbit polyclonal anti-Erk1/2 (#9102; Cell Signaling Technology), mouse monoclonal anti-pTrk (sc-8058; Santa Cruz Biotechnology), mouse monoclonal anti-TrkB (sc-377218; Santa Cruz Biotechnology), mouse monoclonal anti-GLI-2 (sc-271786; Santa Cruz Biotechnology), rabbit monoclonal anti-non-phospho (active) β-catenin (#8814; Cell Signaling Technology), and mouse monoclonal anti-β-actin (A2228; Sigma-Aldrich). The secondary antibodies used were horseradish peroxidase rabbit anti-goat, goat anti-mouse, and goat anti-rabbit (Thermo Fisher Scientific).

Real-Time RT-PCR Analysis

VGF overexpression in the cerebellum was confirmed by real-time RT-PCR analysis. Samples were collected from whole cerebella of VGF-overexpressing mice and WT mice using the method described for western blot analysis. Total RNA was isolated according to the manufacturer's protocol for NeuroSpin RNA II (TAKARA BIO, Shiga, Japan). First-strand cDNA was synthesized from total RNA in a 20 μL reaction mixture using PrimeScript RT reagent Kit (TAKARA). Real-time RT-PCR was performed with a Thermal Cycler Dice Real Time System II (TAKARA) using SYBR Premix Ex Taq II (TAKARA). The PCR protocol consisted of a 30 s denaturation step at 95 °C, followed by a two-step PCR comprising 5 s at 95 °C and 30 s at 60 °C, with 40 cycles for VGF and β-actin. For VGF, the forward primer was 5′-CAGGCTCGAATGTCCGAAAG-3′ and the reverse primer was 5′-CTTGGATAAGGGTGTCAAAGT CTCA-3′. For β-actin, the forward primer was 5′-CATCCG

TAAAGACCTCTATGCCAAC-3′, and the reverse primer was 5′-ATGGAGCCACCGATCCACA-3′. Quantitative real-time RT-PCR analysis was performed using a Thermal Cycler Dice Real Time System TP 800 (TAKARA).

Tissue Preparation

Adult mice and postnatal day 3 mice were anesthetized by sodium pentobarbital (50 mg/kg) or cold anesthesia, respectively, and perfused with saline until the outflow became clear. The perfusate was then changed to 0.1 M phosphate buffer (PB; pH 7.4) containing 4% paraformaldehyde (Wako, Osaka, Japan). The brain was quickly removed and kept immersed for at least 24 h at 4 °C in the same fixative. The brain was equilibrated in 25% sucrose solution and quickly frozen in Tissue-Tek OCT. For histological analysis except for volume and immunostaining of NeuN, phaspho-Histone H3 (pHH3), brain lipid binding protein (BLBP), and Ki67, 10-μm-thick sagittal sections of brain were cut on a cryostat. For consistently, frozen sections analyzed from the cerebellar vermis were limited to the most medial 250 μm. The cerebellar hemisphere was identified as lateral sections within 250 μm after loss of tenth folia of vermis. For histological analysis of cerebellar volume of adult mice and immunostaining of calbindinD28K, 50-μm-thick sagittal sections of brain were cut on a cryostat. The sections were mounted on microslide glass (Matsunami Glass, Osaka, Japan).

Nissl Staining and Histological Analysis

For histological analysis of adult mice, we used frozen cerebellar sagittal sections of vermis and hemisphere regions. For histological analysis of postnatal day 3 mice, we used frozen cerebellar sagittal sections of the vermis region. For measurement of cerebellar volume of adult mice, we applied Cavalieri's principle ($\text{volume} = s_1d_1 + s_2d_2 + \ldots + s_nd_n$, s = area, d = distance between two sections) with 250 μm between the section [37, 38]. Nissl-stained sagittal sections were prepared and outlined from lateral 0.875 mm to lateral 2.725 mm. Frozen sections were stained in cresyl violet for 20 min and dehydrated using absolute ethanol and xylene. Images were taken under a fluorescence microscope (BZ-X710; Keyence, Osaka, Japan). The measurements of the cerebellar sagittal section area were performed using ImageJ software (National Institutes of Health, Bethesda, MD, USA).

Immunohistochemistry of Cerebellar Sections

We used frozen cerebellar sagittal sections of the vermis region. For all immunohistochemistry except for BLBP, fluorescent staining was performed. The sagittal brain sections were blocked with serum (Vector Labs, Burlingame, CA, USA) for 1 h, and incubated with the primary antibody at 4 °C overnight. For the mouse primary antibody, M.O.M immunodetection kits (Vector Labs) were used for blocking and solvents and were incubated with the primary antibody at 4 °C overnight or for 48 h. Then, the sections were incubated with a secondary antibody for 1 or 2 h, counterstained for 10 min using Hoechst 33342 [1:1000 dilution (Thermo Fisher Scientific)], and mounted in Fluoromount (Diagnostic Biosystems, Pleasanton, CA, USA). For immunostaining of Ki67 and calbindinD28K, 0.3 or 0.5% Triton X-100 (Bio-Rad Labs) was used to improve membrane permeability of the antibody, respectively. For immunohistochemistry of BLBP, DAB staining was performed. The sagittal brain sections were treated with 0.3% hydrogen peroxidase in 10% methanol. They were then blocked with serum (Vector Labs). Next, they were incubated with anti-BLBP antibody 4 °C overnight. After that, sections were incubated with biotinylated secondary antibody for 1 h, and then with avidin–biotin peroxidase (Vector Labs) for 30 min. Finally, they were treated with DBA, and then dehydrated using absolute ethanol and xylene. The following antibodies were used: mouse anti-calbindinD28K [1:250 dilution (C9848; Sigma-Aldrich)], rabbit anti-BLBP [1:300 dilution (ABN14; Merck Millipore, Burlington, MA, USA)], mouse anti-NeuN [1:100 dilution (MAB377; Merck Millipore)], mouse anti-pHH3 antibody [1:500 dilution (#9706; Cell Signaling Technology)], rabbit anti-Ki67 antibody [1:100 dilution (AB9260; Merck Millipore)], Alexa Fluor® 546 goat anti-mouse IgG [1:1000 dilution (A11018; Thermo Fisher Scientific)], Alexa Fluor® 488 rabbit anti-mouse IgG [1:1000 dilution (A21204; Thermo Fisher Scientific)], Alexa Fluor® 488 goat anti-rabbit IgG [1:1000 dilution (A11008; Thermo Fisher Scientific)], and biotinylated goat anti-rabbit IgG [1:200 dilution (Vector Labs)]. Images were taken using a fluorescence microscope (BZ-X710; Keyence) or a confocal microscope (FLUOVIEW FV10i; Olympus, Tokyo, Japan). The cell number and density of calbindinD28K$^+$ cell were measured throughout the entire cerebellum. The length of purkinje cell dendrites was measured at eight similar sites per each mouse. The numbers of NeuN$^+$ and pHH3$^+$ cells were measured between the sixth and ninth folia (posterior lobules). The measurement of the rate of Ki67$^+$ cells into Hoechst$^+$ all cells was measured at the midpoint of the eighth and ninth folia.

Granule Cell Precursor Culture

GCPs were isolated from cerebella of WT and VGF-overexpressing mice at P4 and cultured as previously described, except a Percoll gradient separation with minor modification [39]. Briefly, freshly dissected cerebella were placed in HBSS-glucose in a 15 mL conical tube as soon as dissected. Then, cerebella were dissociated using papain

solution. Cells were filtered through a 70-μm nylon mesh, harvested in dishes coated with 100 μg/mL poly-D-lysine (Sigma-Aldrich), and then incubated for 20 min. After gentle tapping of the dish, loosely adhered granule neurons and neuron progenitor cells were separated with astroglia and heavier cells, which settle and adhere to the dish. These separated cells were plated at a density of 3.5×10^4 cells/well in 96-well tissue culture plate coated with 100 μg/mL poly-D-lysine for BrdU immunostaining, and 3.5×10^5 cells/well in glass chamber slides coated with 100 μg/mL of poly-D-lysine for Math1 immunostaining in neurobasal medium (Thermo Fisher Scientific), including GlutaMax I (Thermo Fisher Scientific), B27 supplement (Thermo Fisher Scientific), and antibiotics. Math1 immunostaining was started 3 h after cell seeding. BrdU was added to each well to a final concentration of 10 μM 27 h after cell seeding. Twenty-four hours after BrdU addition, BrdU immunostaining was started. For immunostaining, GCPs derived from WT and VGF-overexpressing mice were used. The measurements were performed using ImageJ software (National Institutes of Health).

In Vitro Immunostaining

The primary cell cultures were fixed with 4% paraformaldehyde at room temperature for 15 min. The cells were pre-treated for 30 min with 2 M hydrochloric acid (HCl), incubated with 0.3% Triton X-100 (Bio-Rad Labs) for 10 min, and treated with 0.1 or 0.05% trypsin (Wako) immediately. Then, cells were incubated with 50 mM glycine in PBS for 15 min. The cells were blocked with 3% goat serum (Vector Labs) for 30 min and incubated with rat anti-BrdU antibody or mouse anti-Math1 antibody (ab6326; abcam, Cambridge, MA, USA, sc-136173; santa cruz) overnight at 4 °C. Then, the cells were incubated for 1 h with Fluor®546 goat anti-rat IgG or Fluor®546 goat anti-mouse IgG and counterstained with Hoechst33342 (Thermo Fisher Scientific). Images were taken using a fluorescence microscope (Keyence) or a confocal microscope (Olympus). For quantitative data of BrdU staining, the entire area of the image was obtained. The number of immunoreactive cells was counted and calculated as the ratio of immunoreactive cells to total cells and normalized to the results of the WT mice.

Rotarod Test

An accelerating rotarod (Ugo Basile, Gemonio, Italy) was used for testing motor coordination. The rotarod speed was set to accelerate from 4 to 40 rpm over 5 min. Latency to fall of each mouse was measured. On the first day, mice were initially placed on the rotating drum (5 rpm) twice for 2 min (training session). One day after the training session, the mice were tested in four trials during day 1, followed by three trials on days 2 and 3.

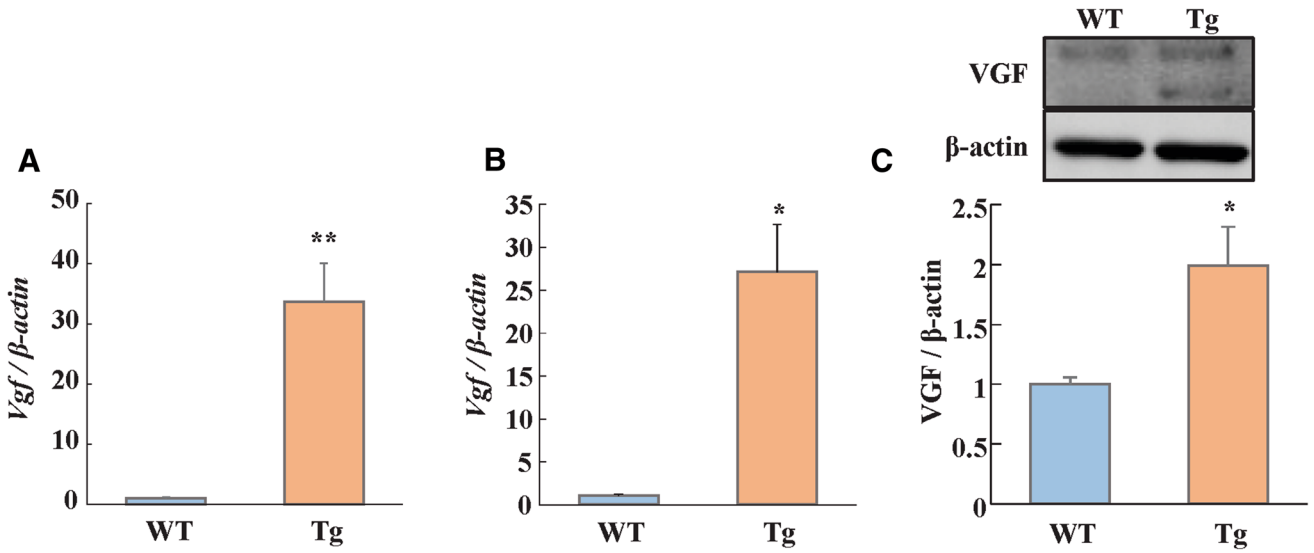

Fig. 1 Upregulation of VGF in the cerebella of VGF-overexpressing mice. **a** The expression level of *Vgf* mRNA in adult mice (8–18 weeks old) relative to the *β-actin* level evaluated by real-time RT-PCR. Data are expressed as the mean fold difference versus WT mice ± SEM (n = 5 or 6). $^{**}P < 0.01$ versus WT mice (Student's *t* test). **b** The expression level of *Vgf* mRNA during the developmental period (postnatal day 3) relative to the *β-actin* level evaluated by real-time RT-PCR. Data are expressed as the mean fold difference versus WT mice ± SEM (n = 3 or 6). $^{*}P < 0.05$ versus WT mice (Student's *t* test). **c** Typical bands show VGF and β-actin. The expression level of VGF protein during the developmental period (postnatal day 3) relative to the β-actin level evaluated by western blot analysis. Data are expressed as the mean fold difference versus WT mice ± SEM (n = 8 or 11). $^{*}P < 0.05$ versus WT mice (Student's *t* test). *WT* wild-type

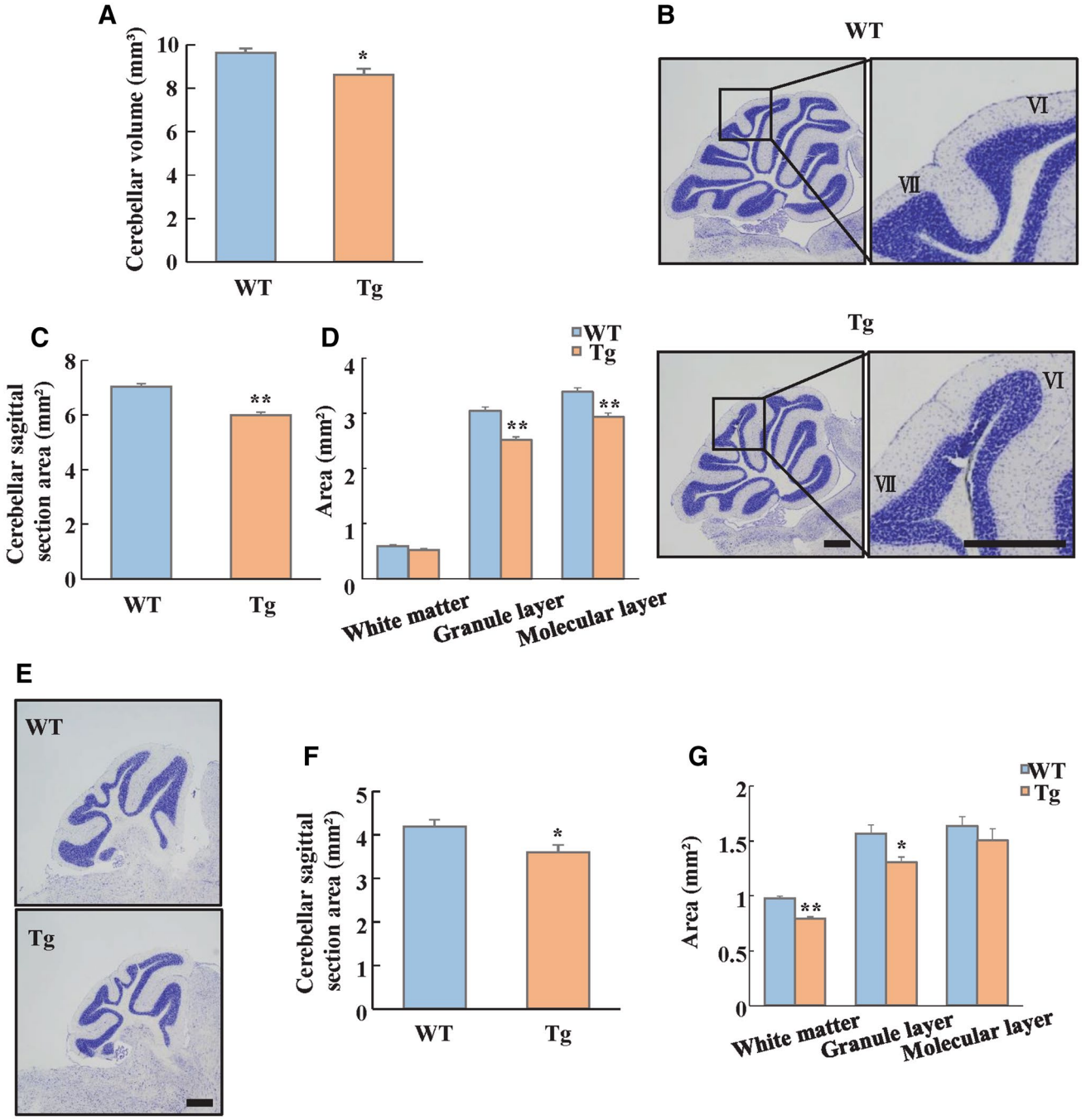

Fig. 2 Histological analysis of the cerebella in adult VGF-overexpressing mice. **a** The cerebellar volume of WT and VGF-overexpressing mice. Data are expressed as the mean ± SEM (n = 4). *$P < 0.05$ versus WT mice (Student's *t* test). **b** Left: Representative images of cerebellar vermis stained with cresyl violet in adult WT and VGF-overexpressing mice. Scale bar = 500 µm. Right: enlarged images of the fissure between the sixth and seventh folia. **c** The cerebellar sagittal section area in the cerebellar vermis of WT and VGF-overexpressing mice. Data are expressed as the mean ± SEM (n = 4). **$P < 0.01$ versus WT mice (Student's *t* test). **d** The cerebellar sagittal section area of white matter, granule layer, and molecular layer of WT and VGF-overexpressing mice. Data are expressed as the mean ± SEM (n = 4). *$P < 0.05$, **$P < 0.01$ versus WT mice (Student's *t* test). **e** Representative images of cerebellar hemispheres stained with cresyl violet in adult WT and VGF-overexpressing mice. Scale bar = 500 µm. **f** The cerebellar sagittal section area in the cerebellar hemispheres of adult WT and VGF-overexpressing mice. Data are expressed as the mean ± SEM (n = 4). *$P < 0.05$ versus WT mice (Student's *t* test). **g** The cerebellar sagittal section area of white matter, granule layer, and molecular layer of adult WT and VGF-overexpressing mice. Data are expressed as the mean ± SEM (n = 4). *$P < 0.05$, **$P < 0.01$ versus WT mice (Student's *t* test). *WT* wild-type

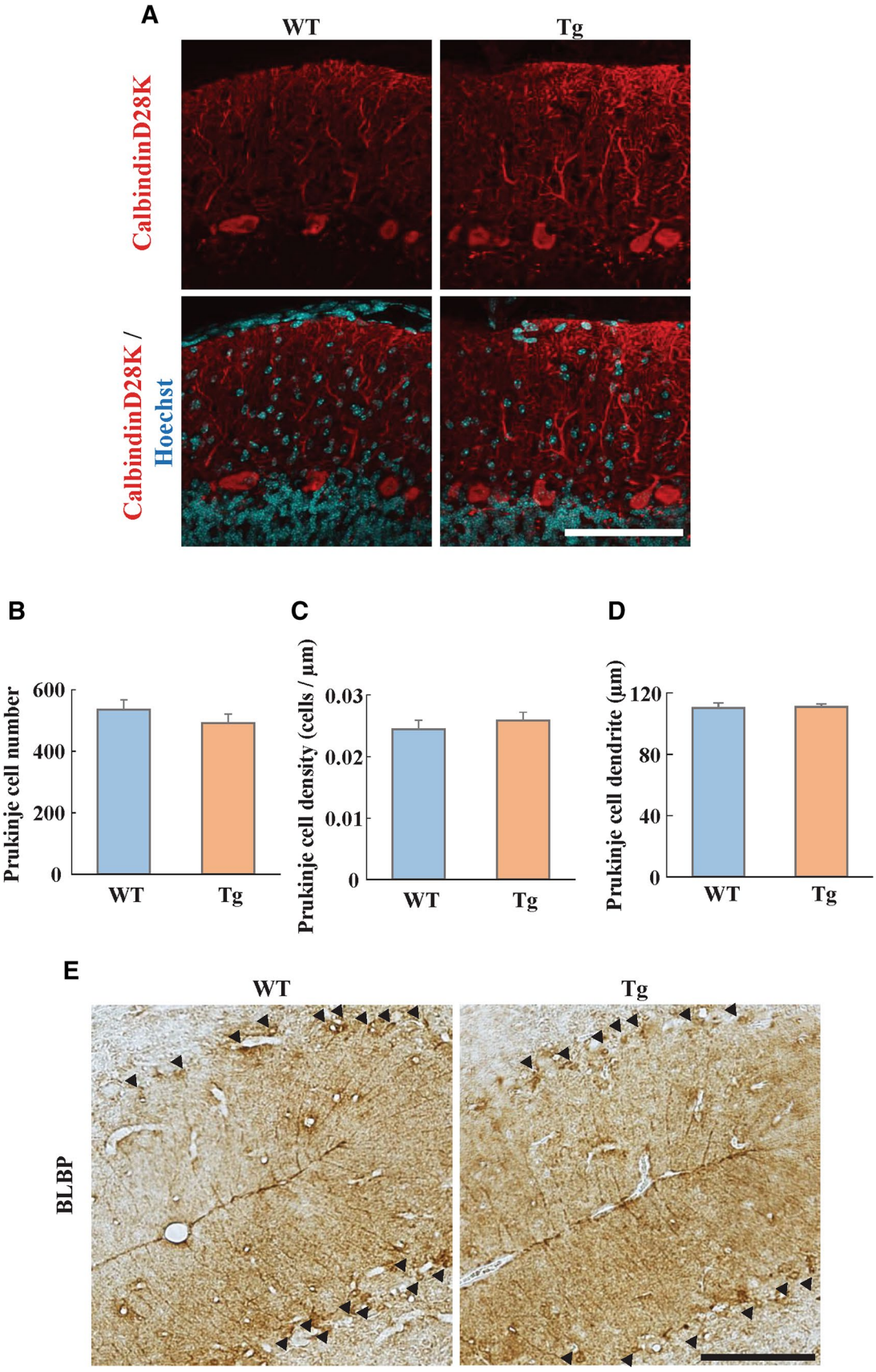
A
WT
Tg
CalbindinD28K
CalbindinD28K / Hoechst
B
Prukinje cell number
600
400
200
0
WT
Tg
C
Prukinje cell density (cells / μm)
0.03
0.02
0.01
0
WT
Tg
D
Prukinje cell dendrite (μm)
120
80
40
0
WT
Tg
E
WT
Tg
BLBP

◂**Fig. 3** Immunohistochemistry of Purkinje cell and Bergmann glia in adult VGF-overexpressing mice. **a** Representative images of calbindinD28K staining in WT and VGF-overexpressing mice. Scale bar = 100 μm. **b** The number of calbindinD28K$^+$ cells in the entire cerebellum of WT and VGF-overexpressing mice. **c** The cell densities of calbindinD28K$^+$ cells in the entire cerebellum of WT and VGF-overexpressing mice. **d** The length of the dendrites in WT and VGF-overexpressing mice. Data are expressed as the mean ± SEM (n = 4). **e** Representative images of BLBP staining in WT and VGF-overexpressing mice. Scale bar = 100 μm. Arrowheads show the BLBP$^+$ Bergmann glia. *BLBP* brain lipid binding protein, *WT* wild-type

Footprint Test

The footprint test was performed to compare the gait of VGF-overexpressing mice and WT mice. The fore- and hindfeet of the mice were coated with red and black nontoxic paints, respectively. The mice were then allowed to walk along a 30-cm-long, 7-cm-wide runway. A fresh sheet of white paper was placed on the floor of the runway for each mouse run. A sequence of five consecutive steps was chosen for evaluation, excluding footprints made at the beginning and end of the run where the animals were initiating and finishing movement, respectively. The same operator (T.M.) blindly conducted all footprint tests. The footprint patterns were analyzed for two parameters: (1) stride lengths of the fore- and hindfeet were measured as the average distance and (2) fore- and hindfeet widths were measured as the average distance between the left and right footprints.

Statistical Analysis

All values are expressed as mean ± standard error. Statistical comparisons were made using a two-tailed Student's *t* test with SPSS Statistics (IBM, Armonk, NY, USA) software. *P* values less than 0.05 were considered statistically significant.

Results

Overexpression of VGF in VGF-Overexpressing Mice During Adult and Developmental Stages

In our previous study, we demonstrated that VGF-overexpressing mice exhibited overexpression of VGF in several brain regions, including the prefrontal cortex, cerebral cortex, hippocampus, and striatum. In the present study, we confirmed overexpression of *Vgf* mRNA and VGF protein during both adult and developmental stages. In adult VGF-overexpressing mice, the expression level of *Vgf* mRNA was higher than that of WT mice (Fig. 1a). Additionally, *Vgf* mRNA and VGF protein levels were higher than those of WT mice during postnatal day 3 (Fig. 1b, c).

Histological Analysis of the Cerebellum in Adult VGF-Overexpressing Mice

We performed a histological analysis of the cerebellum with Nissl staining. At first, we measured cerebellar volume in VGF-overexpressig mice and WT mice. The cerebellar volume from vermis to hemisphere region of VGF-overexpressing mice was significantly decreased compared to WT mice (Fig. 2a). The cerebellum consists of two regions, the vermis and hemisphere. We performed a histological analysis of both the vermis (Fig. 2b–d) and hemisphere (Fig. 2e–g). The cerebellar sagittal section area of VGF-overexpressing mice was smaller than WT mice in both vermis and hemisphere regions (Fig. 2b–g). Interestingly, the cerebella of VGF-overexpressing mice were missing the intercrural fissure between lobules VI and VII, which was a clear abnormality during the histological analysis (Fig. 2b). The missing the intercrural fissure between lobules VI and VII was found in all VGF-overexpressing mice (4 of 4 mice). The cerebellum has a clear layer structure including the molecular layer, Purkinje cell layer, granule layer, and white matter. We performed a detailed histological analysis. The results showed the cerebellar sagittal section area reduction of the granule layer of VGF-overexpressing mice was confirmed in both of vermis and hemisphere regions (Fig. 2d, g). In term of Purkinje cell immunostained with calbindinD28K, there were no significant differences in the cell number, the cell density, and the length of cell dendrites (Fig. 3a–d). In term of Bergmann glia immunostained BLBP, Bergmann glia of both WT and VGF-overexpressing mice formed a monolayer structure in the Purkinje cell layer (Fig. 3e). Additionally, the fibers of Bergmann glia of both WT and VGF-overexpressing mice had an exclusively radial orientation (Fig. 3e). Taken together, there were no significant differences on the morphologies of Purkinje cell and Bergmann glia between WT and VGF-overexpressing mice.

Defective Granule Cell Development of VGF-Overexpressing Mice

Because the area reduction of the granule layer in VGF-overexpressing mice was confirmed in both of vermis and hemisphere regions, and there were no differences on the morphology of Purkinje cell and Bergmann glia, we focused on granule cell development using frozen sections of postnatal day 3 mice. First, we performed cerebellar histological analysis in postnatal day 3 with Nissl staining. The cerebellar sagittal section area of whole cerebellum and external granule layer (EGL), in which GCPs are located, of VGF-overexpressing mice were smaller than that of WT mice (Fig. 4a, b). Moreover, we performed immunohistochemistry with neuronal marker NeuN, which labels all post-mitotic

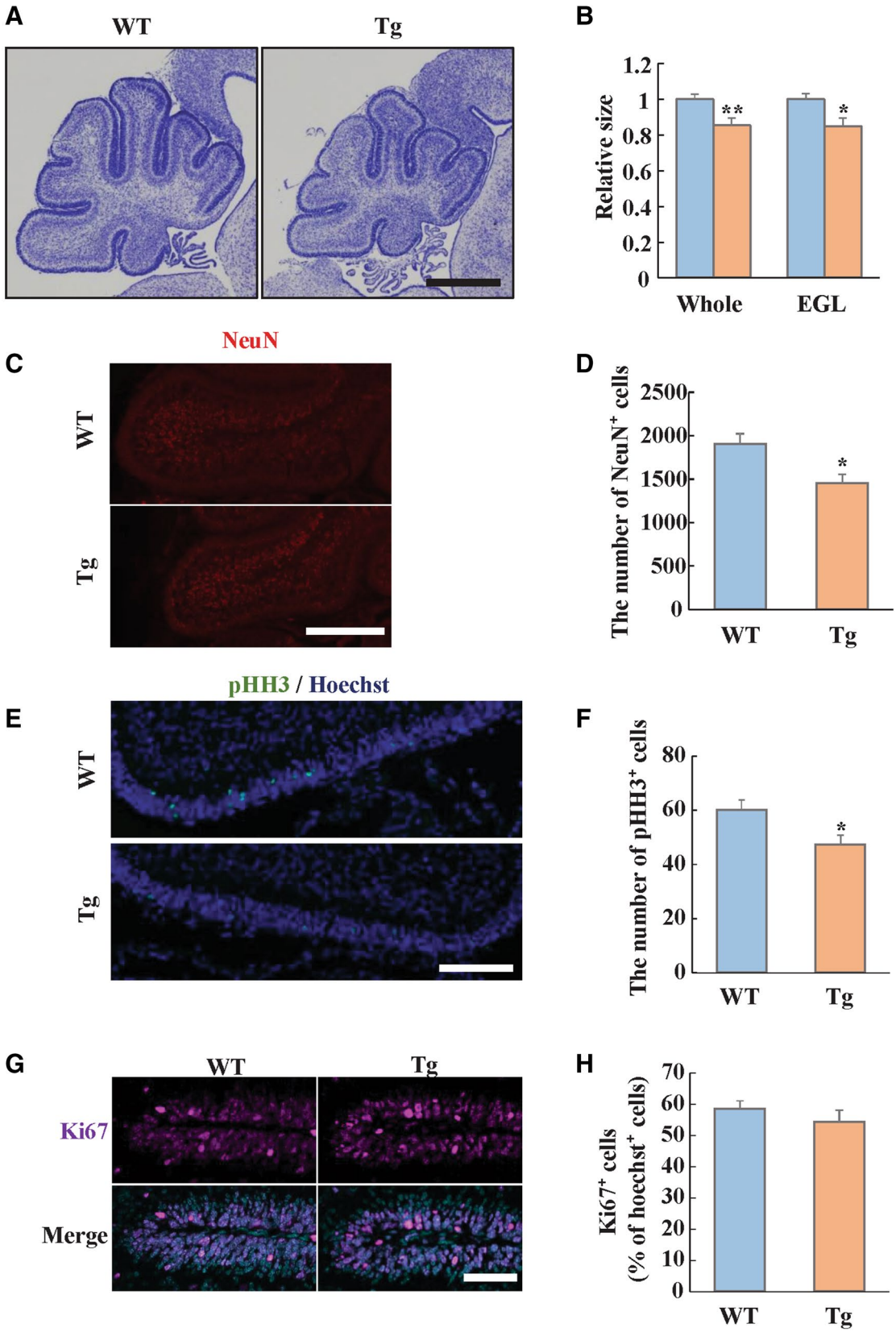
A
WT
Tg
B
Relative size
1.2
1
0.8
0.6
0.4
0.2
0
**
*
Whole
EGL
NeuN
C
WT
Tg
D
The number of NeuN+ cells
2500
2000
1500
1000
500
0
*
WT
Tg
pHH3 / Hoechst
E
WT
Tg
F
The number of pHH3+ cells
80
60
40
20
0
*
WT
Tg
G
WT
Tg
Ki67
Merge
H
Ki67+ cells
(% of hoechst+ cells)
70
60
50
40
30
20
10
0
WT
Tg

◂**Fig. 4** Changes in the development of the cerebellum in VGF-overexpressing mice. **a** Representative images of cerebellar vermis stained with cresyl violet in postnatal day 3 of WT and VGF-overexpressing mice. Scale bar = 500 µm. **b** The cerebellar sagittal section area of the whole cerebellum and EGL in postnatal day 3 of WT and VGF-overexpressing mice. Data are expressed as the mean ± SEM (n = 8 or 10). *$P < 0.05$ versus WT mice (Student's *t* test). **c, d** NeuN staining (red) shows the differentiated granule cells in the IGL of WT and VGF-overexpressing mice. **c** Representative images of NeuN staining in WT and VGF-overexpressing mice. Scale bar = 250 µm. **d** The number of NeuN$^+$ cells in the IGL. Data are expressed as the mean ± SEM (n = 3 or 4). *$P < 0.05$ versus WT mice (Student's *t* test). **e, f** pHH3 staining (green) shows proliferating GCPs in the EGL. **e** Representative images of pHH3 staining in WT and VGF-overexpressing mice. Scale bar = 100 µm. **f** The number of pHH3$^+$ cells in the EGL. Data are expressed as the mean ± SEM (n = 8 or 10). *$P < 0.05$ versus WT mice (Student's *t* test). **g, h** Ki67 staining (magenta) shows GCPs in the EGL. **g** Representative images of Ki67 staining in WT and VGF-overexpressing mice. Scale bar = 50 µm. **h** The percentage of Ki67$^+$ cells into Hoechst$^+$ all cells tin the EGL. Data are expressed as the mean ± SEM (n = 8 or 10). *EGL* external granule layer, *GCP* granule cell precursor, *IGL* internal granule layer, *pHH3* phospho histone H3, *WT* wild-type. (Color figure online)

neurons except for Purkinje cells [40] in the internal granule layer (IGL). The number of NeuN$^+$ cells in the IGL of VGF-overexpressing mice was decreased than that of WT mice (Fig. 4c, d). These results suggest that VGF-overexpressing mice exhibit the hypoplasia of granule layer during developmental stage. To investigate the causes of cerebellar hypoplasia, we measured the change in degree of proliferation and differentiation between VGF-overexpressing mice and WT mice. To determine the degree of proliferation, we performed immunohistochemistry with M phase proliferating marker pHH3. The number of pHH3$^+$ cells in the EGL of VGF-overexpressing mice was decreased compared with WT mice (Fig. 4e, f). During the developmental stage, proliferating GCPs are in the outer region of the EGL and express Ki67 [41]. After mitotic division, GCPs differentiate into immature granule cells, which accumulate in the inner EGL and express Tuj1 [42]. Therefore, degree of differentiation can be measured by the rate of Ki67-positive cells in all cells in EGL [43]. To investigate the degree of differentiation of GCPs of VGF-overexpressing mice, we performed immunohistochemistry with Ki67 antibody. Ki67$^+$ cells were in the outer EGL in both VGF-overexpressing and WT mice (Fig. 4g). Moreover, there was no difference of the rate of Ki67$^+$ cells into Hoechst$^+$ all cells in the EGL between VGF-overexpressing mice and WT mice (Fig. 4h). Therefore, there was no change on the degree of the differentiation between WT and VGF-overexpressing mice.

Change of Proliferation Relating Signal of the Developmental Cerebellum in VGF-Overexpressing Mice

In previous reports, VGF-derived peptide (TLQP-62) reinforced BDNF–TrkB signaling in the hippocampus [6, 7]. Moreover, BDNF and its downstream factor, Erk, is involved in the proliferation and differentiation of GCPs [6, 7, 33, 44]. To investigate the expression change, we performed western blotting of Trk–Erk signaling. In postnatal day 3, in the cerebella of VGF-overexpressing mice, phosphorylation of Trk and Erk1 were promoted (Fig. 5a, b). There was no change in Wnt–β-catenin and sonic hedgehog signaling between WT and VGF-overexpressing mice (Fig. 5c).

Reduction of Potential Proliferation of GCPs in Primary Culture

We investigated the degree of proliferation of GCPs in VGF-overexpressing primary cell cultures derived from WT and VGF-overexpressing mice. We confirmed the abundance of GCPs in these culture by immunostaining of Math1 (GCPs marker). In this experiment, the majority of primary cultures were Math1$^+$ cells as the Fig. 6a indicated. The percentage of BrdU$^+$ cells was lower than that of WT mice (Fig. 6b, c).

Impaired Motor Coordination of VGF-Overexpressing Mice

Finally, we investigated whether developmental deficits of granule cells influenced cerebellar functions in life. As abnormal cerebellar development is often associated with a motor coordination deficit, we performed the rotarod test (Fig. 7a) and footprint test (Fig. 7b, c). In the rotarod test, adult VGF-overexpressing mice fell early from the rod during all trials compared with WT mice (Fig. 7a). In the footprint test, VGF-overexpressing mice had a larger hindfeet width and shorter front feet stride compared with WT mice (Fig. 7b, c). These results demonstrate that VGF-overexpressing mice exhibit a motor coordination deficit.

Discussion

Developmental disabilities of the brain are implicated in the pathology of several mental illnesses, including schizophrenia and autism [15–17]. In previous reports, VGF enhanced neurogenesis in cultured hippocampal neurons, and promoted dendritic growth of cultured cortical neurons [7, 29, 30]. However, how VGF influences the development of the immature brain in vivo is still unknown. In the present study, we first demonstrated that VGF may be implicated in the neural development of the cerebellum in vivo. We found that

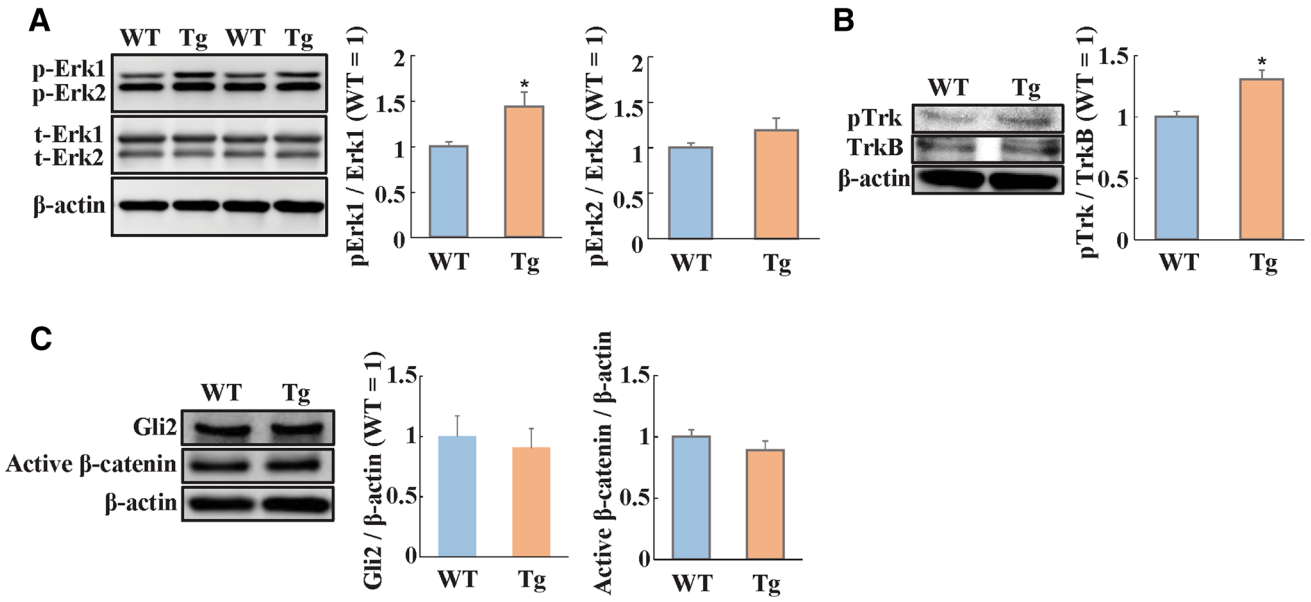

Fig. 5 The expression changes of MAPK, Wnt, and Shh signaling in VGF-overexpressing mice during the developmental period. **a** Representative images show pErk, Erk, and β-actin. The quantitative data show the expression pErk1 and pErk2 during the developmental period relative to Erk1 and Erk2 levels. Data are expressed as the fold difference versus WT mice ± SEM (n = 8 or 11). *$P < 0.05$ versus WT mice (Student's *t* test). **b** Representative images show pTrk, TrkB, and β-actin. The quantitative data show the expression pTrk during the developmental period relative to the TrkB level. Data are expressed as the fold difference versus WT mice ± SEM (n = 3 or 6). *$P < 0.05$ versus WT mice (Student's *t* test). **c** Representative images show Gli2, active β-catenin, and β-actin. The quantitative data show the expression Gli2 and active β-catenin during the developmental period relative to the β-actin level. Data are expressed as the fold difference versus WT mice ± SEM (n = 8 or 11). *WT* wild-type

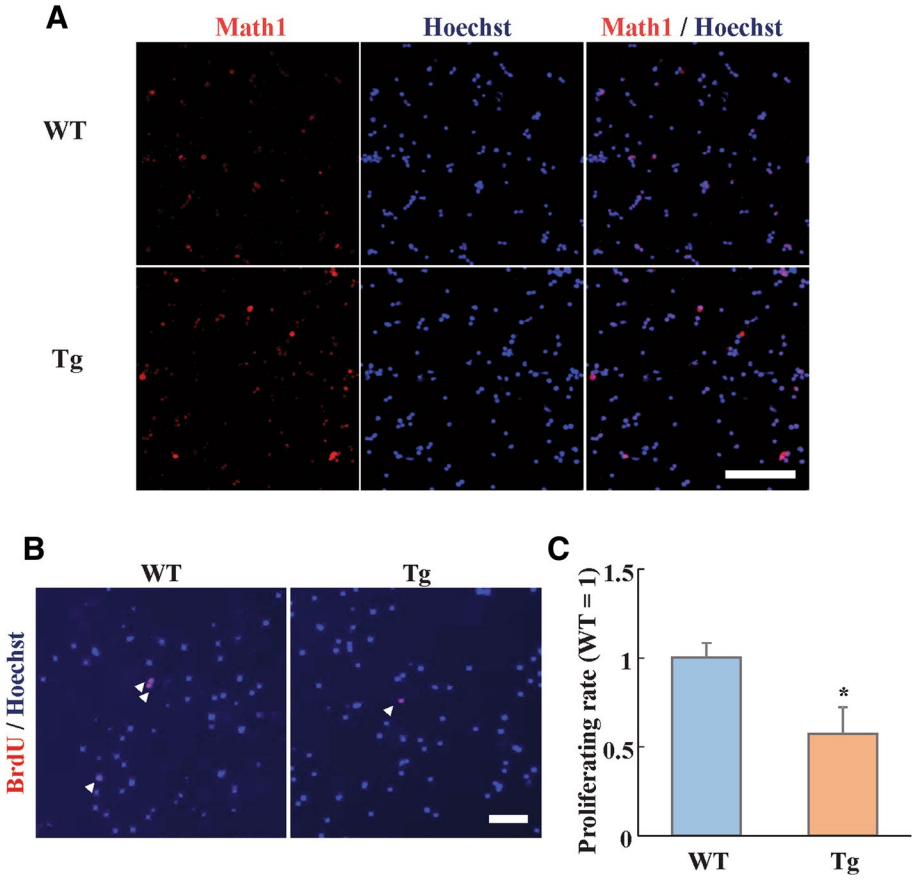

Fig. 6 Reduction of potential proliferation in GCPs of VGF-overexpressing mice. **a** Representative images of Math1 staining in WT and VGF-overexpressing mice. Scale bar = 100 μm. **b** Representative images show proliferating cells (red by BrdU expression) in WT and VGF-overexpressing mice. Nuclei are blue by Hoechst 33342 staining. Scale bar = 500 μm. **c** The quantitative data shows the percentage of $BrdU^+$ cells in WT and VGF-overexpressing mice. Arrowheads show the $BrdU^+$ cells. Data are expressed as the fold difference versus WT mice ± SEM (n = 6 or 7). *$P < 0.05$ versus WT mice (Student's *t* test). *BrdU* 5-bromo-2′-deoxyuridine, *GCP* granule cell precursor, *WT* wild-type. (Color figure online)

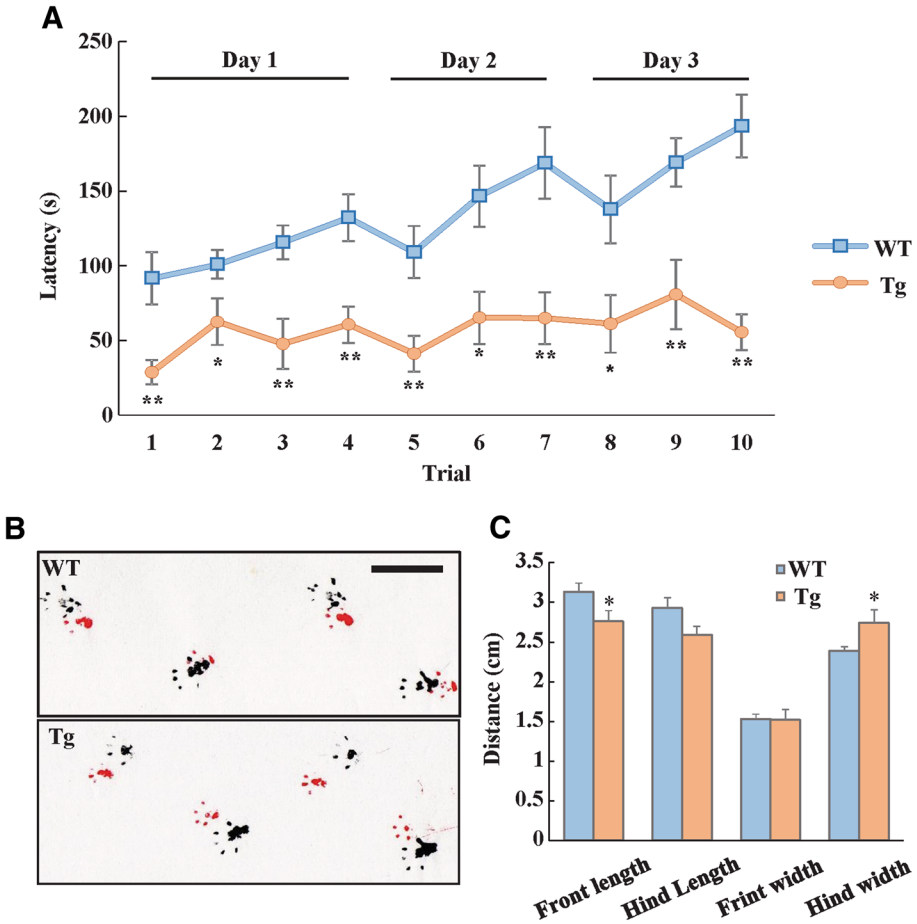

Fig. 7 Ataxic phenotypes of VGF-overexpressing mice. **a** Latency to fall of WT and VGF-overexpressing mice. Data are expressed as the mean ± SEM (n = 8 or 10). *$P < 0.05$, **$P < 0.01$ versus WT mice (Student's *t* test). **b** Representative images of the footprint test in WT and VGF-overexpressing mice. Scale bar = 2 cm. **c** The stride length and base width of front and hind feet. Data are expressed as the mean ± SEM (n = 8 or 10). *$P < 0.05$ versus WT mice (Student's *t* test). *WT* wild-type

VGF-overexpressing mice exhibited cerebellar hypoplasia, developmental impairment of granule cells, and increased phosphorylation of Trk and Erk in the developmental cerebellum, which was accompanied by motor dysfunction.

The cerebellum has a laminar structure including a molecular layer, Purkinje cell layer, granule layer, and white matter, and is convenient for performing morphological analyses. Generally, the cerebellum is subdivided into the vermis and hemisphere regions. The cerebellar vermis has ten major lobules (I–X anterior to posterior) [45]. The cerebellar hemisphere has four lobules (Simplex, Crus I, Crus II, and Paramedian) [45]. In the present study, we focused on the development of granule cells, which are the main cells in the granule layer. In the developmental stage of mice, GCPs derived from the rhombic lip migrate to the anlage of the developing cerebellum and form the EGL [46]. In this layer, GCPs in the EGL proliferate and subsequently exit the cell cycle. Moreover, these cells migrate toward the inner granule layer to form the adult granule layer. The EGL is subdivided into two areas; an upper, mitotically active (outer EGL) and a lower, migratory layer (inner EGL) [47]. In our in vivo and in vitro studies, the proliferation of GCPs in VGF-overexpressing mice was low; however, the differentiation was not changed. As the mechanism underlying the VGF-overexpressing phenotype, the phosphorylation of Trk and Erk were promoted. Trk is the receptor of several neurotrophic factors, including BDNF and NT-3 [48]. In the developmental brain, expression of *trk*A mRNA was weaker than those of *trk*B and *trk*C, and the best correlation was found between the VGF and *trk*B [49]. Therefore, it is suggested that the promotion of the phosphorylation of Trk is most depend on TrkB. Previous reports demonstrated that these neurotrophic factors promote differentiation and migration of GCPs, and maturation and maintenance of differentiated granule cells [50–53]. Additionally, in $BDNF^{-/-}$ mice and $CAPS2^{-/-}$ mice, the differentiation of GCPs was delayed, and the EGL was thick when it was barely detectable in the WT mice [52, 53]. When cells differentiate, the cell cycle stops and the proliferation potency decreases [54]. Based on these reports, neurotrophic factors promote exit of the cell cycle and differentiation of GCPs into granule neurons. Erk is downstream of the Ras/Raf/MEK/ERK signaling cascade. Many reports demonstrate that ERK activation is involved with the promotion or inhibition of cell proliferation bilaterality in several cells [55]. Others

have reported that the activation of Erk suppresses GCPs proliferation via RAS and Wnt3 [33, 44]. Taken together, these previous reports and our present results suggest that VGF has a suppressing effect on the proliferation of GCPs via phosphorylation of Trk and Erk.

In addition to impaired cerebellar development, VGF-overexpressing mice exhibited impaired motor coordination and ataxic gait, whose impairment was confirmed in mice with a cerebellar disability [34, 56]. Although VGF-overexpressing mice exhibited normal cerebellar patterning, the development of granule cell precursors was impaired. The impairment of development of granule cells influences cerebellar circuity [57]. Taken together, VGF-overexpressing mice have impaired development of GCPs, which impacts cerebellar circuity and motor function. However, future works should investigate cerebellar circuity using electrophysiological techniques. Further, our previous study demonstrated that VGF-overexpressing mice exhibited striatal morphological defects, whose function is important for motor coordination [13]. Thus, both cerebellar morphological defects and those of the striatum are responsible for impaired motor coordination and ataxic gait in VGF-overexpressing mice.

In conclusion, we demonstrated that increased VGF expression promoted Trk/Erk signaling (which is important for neural proliferation, differentiation, and maturation), impaired granule cell development, and resulted in motor disability in adult mice.

Acknowledgements This work was supported by JSPS KAKENHI Grant Number JP18J14970.

Compliance with Ethical Standards

Conflict of interest The author declare that they have no competing interest.

References

1. Trani E, Giorgi A, Canu N, Amadoro G, Rinaldi AM, Halban PA, Ferri GL, Possenti R, Schinina ME, Levi A (2002) Isolation and characterization of VGF peptides in rat brain. Role of PC1/3 and PC2 in the maturation of VGF precursor. J Neurochem 81:565–574
2. Bartolomucci A, La Corte G, Possenti R, Locatelli V, Rigamonti AE, Torsello A, Bresciani E, Bulgarelli I, Rizzi R, Pavone F, D'Amato FR, Severini C, Mignogna G, Giorgi A, Schinina ME, Elia G, Brancia C, Ferri GL, Conti R, Ciani B, Pascucci T, Dell'Omo G, Muller EE, Levi A, Moles A (2006) TLQP-21, a VGF-derived peptide, increases energy expenditure and prevents the early phase of diet-induced obesity. Proc Natl Acad Sci USA 103:14584–14589
3. Levi A, Eldridge JD, Paterson BM (1985) Molecular cloning of a gene sequence regulated by nerve growth factor. Science 229:393–395
4. Alder J, Thakker-Varia S, Bangasser DA, Kuroiwa M, Plummer MR, Shors TJ, Black IB (2003) Brain-derived neurotrophic factor-induced gene expression reveals novel actions of VGF in hippocampal synaptic plasticity. J Neurosci 23:10800–10808
5. Bonni A, Ginty DD, Dudek H, Greenberg ME (1995) Serine 133-phosphorylated CREB induces transcription via a cooperative mechanism that may confer specificity to neurotrophin signals. Mol Cell Neurosci 6:168–183
6. Lin WJ, Jiang C, Sadahiro M, Bozdagi O, Vulchanova L, Alberini CM, Salton SR (2015) VGF and its C-terminal peptide TLQP-62 regulate memory formation in hippocampus via a BDNF-TrkB-dependent mechanism. J Neurosci 35:10343–10356
7. Thakker-Varia S, Behnke J, Doobin D, Dalal V, Thakkar K, Khadim F, Wilson E, Palmieri A, Antila H, Rantamaki T, Alder J (2014) VGF (TLQP-62)-induced neurogenesis targets early phase neural progenitor cells in the adult hippocampus and requires glutamate and BDNF signaling. Stem Cell Res 12:762–777
8. Bozdagi O, Rich E, Tronel S, Sadahiro M, Patterson K, Shapiro ML, Alberini CM, Huntley GW, Salton SR (2008) The neurotrophin-inducible gene Vgf regulates hippocampal function and behavior through a brain-derived neurotrophic factor-dependent mechanism. J Neurosci 28:9857–9869
9. Walsh T, McClellan JM, McCarthy SE, Addington AM, Pierce SB, Cooper GM, Nord AS, Kusenda M, Malhotra D, Bhandari A, Stray SM, Rippey CF, Roccanova P, Makarov V, Lakshmi B, Findling RL, Sikich L, Stromberg T, Merriman B, Gogtay N, Butler P, Eckstrand K, Noory L, Gochman P, Long R, Chen Z, Davis S, Baker C, Eichler EE, Meltzer PS, Nelson SF, Singleton AB, Lee MK, Rapoport JL, King MC, Sebat J (2008) Rare structural variants disrupt multiple genes in neurodevelopmental pathways in schizophrenia. Science 320:539–543
10. Rodriguez-Santiago B, Brunet A, Sobrino B, Serra-Juhe C, Flores R, Armengol L, Vilella E, Gabau E, Guitart M, Guillamat R, Martorell L, Valero J, Gutierrez-Zotes A, Labad A, Carracedo A, Estivill X, Perez-Jurado LA (2010) Association of common copy number variants at the glutathione *S*-transferase genes and rare novel genomic changes with schizophrenia. Mol Psychiatry 15:1023–1033
11. Huang JT, Leweke FM, Oxley D, Wang L, Harris N, Koethe D, Gerth CW, Nolden BM, Gross S, Schreiber D, Reed B, Bahn S (2006) Disease biomarkers in cerebrospinal fluid of patients with first-onset psychosis. PLoS Med 3:e428
12. Huang JT, Leweke FM, Tsang TM, Koethe D, Kranaster L, Gerth CW, Gross S, Schreiber D, Ruhrmann S, Schultze-Lutter F, Klosterkotter J, Holmes E, Bahn S (2007) CSF metabolic and proteomic profiles in patients prodromal for psychosis. PLoS ONE 2:e756
13. Mizoguchi T, Minakuchi H, Ishisaka M, Tsuruma K, Shimazawa M, Hara H (2017) Behavioral abnormalities with disruption of brain structure in mice overexpressing VGF. Sci Rep 7:4691
14. Mizoguchi T, Minakuchi H, Tanaka M, Tsuruma K, Shimazawa M, Hara H (2017) Sensorimotor gating deficits and effects of antipsychotics on the hyperactivity in VGF-overexpressing mice. Pharmacol Rep 70:476–480
15. Hazlett HC, Gu H, Munsell BC, Kim SH, Styner M, Wolff JJ, Elison JT, Swanson MR, Zhu H, Botteron KN, Collins DL, Constantino JN, Dager SR, Estes AM, Evans AC, Fonov VS, Gerig G, Kostopoulos P, McKinstry RC, Pandey J, Paterson S, Pruett JR, Schultz RT, Shaw DW, Zwaigenbaum L, Piven J, Network I, IBIS Network, Clinical Sites, Data Coordinating Center, Image Processing Core, Statistical Analysis (2017) Early brain development in infants at high risk for autism spectrum disorder. Nature 542:348–351
16. Tang G, Gudsnuk K, Kuo SH, Cotrina ML, Rosoklija G, Sosunov A, Sonders MS, Kanter E, Castagna C, Yamamoto A, Yue Z, Arancio O, Peterson BS, Champagne F, Dwork AJ,

Goldman J, Sulzer D (2014) Loss of mTOR-dependent macroautophagy causes autistic-like synaptic pruning deficits. Neuron 83:1131–1143
17. Arnold SE, Talbot K, Hahn CG (2005) Neurodevelopment, neuroplasticity, and new genes for schizophrenia. Prog Brain Res 147:319–345
18. Isshiki M, Tanaka S, Kuriu T, Tabuchi K, Takumi T, Okabe S (2014) Enhanced synapse remodelling as a common phenotype in mouse models of autism. Nat Commun 5:4742
19. Mao Y, Ge X, Frank CL, Madison JM, Koehler AN, Doud MK, Tassa C, Berry EM, Soda T, Singh KK, Biechele T, Petryshen TL, Moon RT, Haggarty SJ, Tsai LH (2009) Disrupted in schizophrenia 1 regulates neuronal progenitor proliferation via modulation of GSK3β/β-catenin signaling. Cell 136:1017–1031
20. Tomita K, Kubo K, Ishii K, Nakajima K (2011) Disrupted-in-Schizophrenia-1 (Disc1) is necessary for migration of the pyramidal neurons during mouse hippocampal development. Hum Mol Genet 20:2834–2845
21. Smith SE, Elliott RM, Anderson MP (2012) Maternal immune activation increases neonatal mouse cortex thickness and cell density. J Neuroimmune Pharmacol 7:529–532
22. Choi GB, Yim YS, Wong H, Kim S, Kim H, Kim SV, Hoeffer CA, Littman DR, Huh JR (2016) The maternal interleukin-17a pathway in mice promotes autism-like phenotypes in offspring. Science 351:933–939
23. Basson MA, Wingate RJ (2013) Congenital hypoplasia of the cerebellum: developmental causes and behavioral consequences. Front Neuroanat 7:29
24. Buckley PF (2005) Neuroimaging of schizophrenia: structural abnormalities and pathophysiological implications. Neuropsychiatr Dis Treat 1:193–204
25. Fukumitsu H, Ohtsuka M, Murai R, Nakamura H, Itoh K, Furukawa S (2006) Brain-derived neurotrophic factor participates in determination of neuronal laminar fate in the developing mouse cerebral cortex. J Neurosci 26:13218–13230
26. Lim SH, Park E, You B, Jung Y, Park AR, Park SG, Lee JR (2013) Neuronal synapse formation induced by microglia and interleukin 10. PLoS ONE 8:e81218
27. Liu B, Zupan B, Laird E, Klein S, Gleason G, Bozinoski M, Gal Toth J, Toth M (2014) Maternal hematopoietic TNF, via milk chemokines, programs hippocampal development and memory. Nat Neurosci 17:97–105
28. Namba H, Nagano T, Jodo E, Eifuku S, Horie M, Takebayashi H, Iwakura Y, Sotoyama H, Takei N, Nawa H (2017) Epidermal growth factor signals attenuate phenotypic and functional development of neocortical GABA neurons. J Neurochem 142:886–900
29. Hunsberger JG, Newton SS, Bennett AH, Duman CH, Russell DS, Salton SR, Duman RS (2007) Antidepressant actions of the exercise-regulated gene VGF. Nat Med 13:1476–1482
30. Sato H, Fukutani Y, Yamamoto Y, Tatara E, Takemoto M, Shimamura K, Yamamoto N (2012) Thalamus-derived molecules promote survival and dendritic growth of developing cortical neurons. J Neurosci 32:15388–15402
31. Rapoport M, van Reekum R, Mayberg H (2000) The role of the cerebellum in cognition and behavior: a selective review. J Neuropsychiatry Clin Neurosci 12:193–198
32. Schutter DJ, van Honk J (2005) The cerebellum on the rise in human emotion. Cerebellum 4:290–294
33. Sanchez-Ortiz E, Cho W, Nazarenko I, Mo W, Chen J, Parada LF (2014) NF1 regulation of RAS/ERK signaling is required for appropriate granule neuron progenitor expansion and migration in cerebellar development. Genes Dev 28:2407–2420
34. Rosin JM, McAllister BB, Dyck RH, Percival CJ, Kurrasch DM, Cobb J (2015) Mice lacking the transcription factor SHOX2 display impaired cerebellar development and deficits in motor coordination. Dev Biol 399:54–67
35. Williams SE, Garcia I, Crowther AJ, Li S, Stewart A, Liu H, Lough KJ, O'Neill S, Veleta K, Oyarzabal EA, Merrill JR, Shih YY, Gershon TR (2015) Aspm sustains postnatal cerebellar neurogenesis and medulloblastoma growth in mice. Development 142:3921–3932
36. Butts T, Green MJ, Wingate RJ (2014) Development of the cerebellum: simple steps to make a 'little brain'. Development 141:4031–4041
37. Dai Y, Dudek NL, Li Q, Fowler SC, Muma NA (2009) Striatal expression of a calmodulin fragment improved motor function, weight loss, and neuropathology in the R6/2 mouse model of Huntington's disease. J Neurosci 29:11550–11559
38. Rauskolb S, Zagrebelsky M, Dreznjak A, Deogracias R, Matsumoto T, Wiese S, Erne B, Sendtner M, Schaeren-Wiemers N, Korte M, Barde YA (2010) Global deprivation of brain-derived neurotrophic factor in the CNS reveals an area-specific requirement for dendritic growth. J Neurosci 30:1739–1749
39. Lee HY, Greene LA, Mason CA, Manzini MC (2009) Isolation and culture of post-natal mouse cerebellar granule neuron progenitor cells and neurons. J Vis Exp. https://doi.org/10.3791/990
40. Mullen RJ, Buck CR, Smith AM (1992) NeuN, a neuronal specific nuclear protein in vertebrates. Development 116:201–211
41. Li P, Du F, Yuelling LW, Lin T, Muradimova RE, Tricarico R, Wang J, Enikolopov G, Bellacosa A, Wechsler-Reya RJ, Yang ZJ (2013) A population of Nestin-expressing progenitors in the cerebellum exhibits increased tumorigenicity. Nat Neurosci 16:1737–1744
42. Qu Q, Smith FI (2005) Neuronal migration defects in cerebellum of the *Large*^{myd} mouse are associated with disruptions in Bergmann glia organization and delayed migration of granule neurons. Cerebellum 4:261–270
43. Zanin JP, Abercrombie E, Friedman WJ (2016) Proneurotrophin-3 promotes cell cycle withdrawal of developing cerebellar granule cell progenitors via the p75 neurotrophin receptor. Elife 5
44. Anne SL, Govek EE, Ayrault O, Kim JH, Zhu X, Murphy DA, Van Aelst L, Roussel MF, Hatten ME (2013) WNT3 inhibits cerebellar granule neuron progenitor proliferation and medulloblastoma formation via MAPK activation. PLoS ONE 8:e81769
45. Cheng Y, Sudarov A, Szulc KU, Sgaier SK, Stephen D, Turnbull DH, Joyner AL (2010) The Engrailed homeobox genes determine the different foliation patterns in the vermis and hemispheres of the mammalian cerebellum. Development 137:519–529
46. Altman J, Bayer SA (1978) Prenatal development of the cerebellar system in the rat. I. Cytogenesis and histogenesis of the deep nuclei and the cortex of the cerebellum. J Comp Neurol 179:23–48
47. Sathyamurthy A, Yin DM, Barik A, Shen C, Bean JC, Figueiredo D, She JX, Xiong WC, Mei L (2015) ERBB3-mediated regulation of Bergmann glia proliferation in cerebellar lamination. Development 142:522–532
48. Huang EJ, Reichardt LF (2003) Trk receptors: roles in neuronal signal transduction. Annu Rev Biochem 72:609–642
49. Snyder SE, Li J, Salton SR (1997) Comparison of VGF and trk mRNA distributions in the developing and adult rat nervous systems. Brain Res Mol Brain Res 49:307–311
50. Schwartz PM, Borghesani PR, Levy RL, Pomeroy SL, Segal RA (1997) Abnormal cerebellar development and foliation in BDNF$^{-/-}$ mice reveals a role for neurotrophins in CNS patterning. Neuron 19:269–281
51. Doughty ML, Lohof A, Campana A, Delhaye-Bouchaud N, Mariani J (1998) Neurotrophin-3 promotes cerebellar granule cell exit from the EGL. Eur J Neurosci 10:3007–3011
52. Borghesani PR, Peyrin JM, Klein R, Rubin J, Carter AR, Schwartz PM, Luster A, Corfas G, Segal RA (2002) BDNF

stimulates migration of cerebellar granule cells. Development 129:1435–1442
53. Sadakata T, Kakegawa W, Mizoguchi A, Washida M, Katoh-Semba R, Shutoh F, Okamoto T, Nakashima H, Kimura K, Tanaka M, Sekine Y, Itohara S, Yuzaki M, Nagao S, Furuichi T (2007) Impaired cerebellar development and function in mice lacking CAPS2, a protein involved in neurotrophin release. J Neurosci 27:2472–2482
54. Ruijtenberg S, van den Heuvel S (2016) Coordinating cell proliferation and differentiation: antagonism between cell cycle regulators and cell type-specific gene expression. Cell Cycle 15:196–212
55. Chambard JC, Lefloch R, Pouyssegur J, Lenormand P (2007) ERK implication in cell cycle regulation. Biochim Biophys Acta 1773:1299–1310
56. Wang JY, Yu IS, Huang CC, Chen CY, Wang WP, Lin SW, Jeang KT, Chi YH (2015) Sun1 deficiency leads to cerebellar ataxia in mice. Dis Model Mech 8:957–967
57. Sadakata T, Kakegawa W, Shinoda Y, Hosono M, Katoh-Semba R, Sekine Y, Sato Y, Saruta C, Ishizaki Y, Yuzaki M, Kojima M, Furuichi T (2014) Axonal localization of Ca^{2+}-dependent activator protein for secretion 2 is critical for subcellular locality of brain-derived neurotrophic factor and neurotrophin-3 release affecting proper development of postnatal mouse cerebellum. PLoS ONE 9:e99524